ACS APPLIED NANO MATERIALS

www.acsanm.org Article

Examination of Nanoparticle Filtration by Filtering Facepiece Respirators During the COVID-19 Pandemic

Junli Hao, Rachel Passos de Oliveira Santos, and Gregory C. Rutledge*

Cite This: https://doi.org/10.1021/acsanm.1c00139 Read Online

ACCESS | Metrics & More | Article Recommendations | Supporting Information

ABSTRACT: The onset of the COVID-19 pandemic in spring 2020 resulted in a spike in the demand for face masks and respirators. Due to their effectiveness at filtering aerosols that could potentially contain viruses, the N95-type filtering facepiece respirators (FFRs) are frequently used by healthcare workers and first responders. However, due to a shortage of domestic N95 FFRs in the US at the beginning of the pandemic, internationally produced respirators were imported and deployed under an Emergency Use Authorization by the Food and Drug Administration. Due to concerns raised at the time, there was an urgent need to verify their effectiveness and usability. In this study, we summarize our characterization of the nanoparticulate filtration performances of 136 such respirators, measured between April 1 and June 30, 2020. Our results indicate that about 42% of the respirators showed filtration efficiencies better than 90% (≤10% penetration), but only 17% performed better than 95% (≤5% penetration). On the other hand, about 35% showed filtration efficiencies below 80% (≥20% penetration). A representative subset of devices was analyzed for the origin of such variations in filtration performance. We found that filtration efficiency increased with the level of electrostatic charge on the FFRs and that the poor performance of the internationally sourced FFRs could be traced to a lack of electrostatic filtration mechanisms. Furthermore, electrostatics shifted the particle size at which aerosol penetration through the FFR was maximal from around 200 nm to less than 100 nm for the highest-performing FFRs, a size range that largely goes undetected in standardized tests.

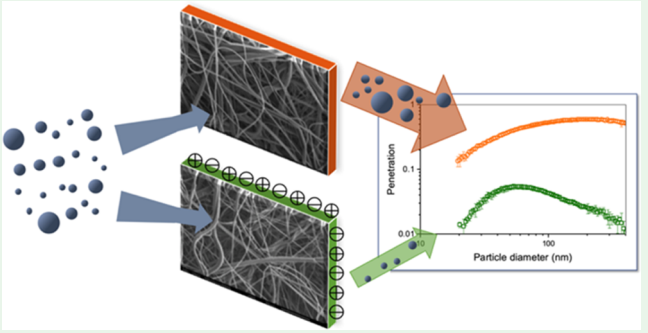

KEYWORDS: *N95, respirator, nanoparticle, aerosol, filtration efficiency, electrostatic, COVID-19*

INTRODUCTION

With the wide spread of SARS CoV-2, the novel coronavirus first identified in December of 2019 and responsible for coronavirus disease 2019 (COVID-19), healthcare personnel and first responders in Massachusetts and other states faced a shortage of personal protective equipment (PPE), such as face masks and respirators, in the spring of 2020. According to the Centers for Disease Control and Prevention (CDC), respiratory viruses can be transmitted through three major modes: contact, droplet, and airborne. During contact transmission, the virus is spread through direct contact with an infectious person or a contaminated article or surface. Droplet transmission refers to the transfer of the virus through respiratory droplets, which generally occurs within close distance (about 6 ft, or 2 m) of an infectious person. Airborne transmission, on the other hand, takes place through smaller virus-containing aerosols (<5 μm diameter) that can remain suspended in air and be transmitted over long periods of time and across distances greater than 2 m.[1,2] In fact, the SARS virus is around 80 nm in diameter, and recent studies demonstrated submicron aerosols to be a plausible mechanism for transmission of COVID-19[3] or even the main mechanism in the case of a Wuhan hospital.[4,5]

The CDC recommends that face coverings be worn in public to reduce the spread of the virus.[6] Among the different types of face coverings, face masks are loose-fitting and largely protect against emissions of large respiratory droplets during exhalation. By contrast, recent studies have shown that the effectiveness of fabric face masks against small airborne aerosols varies significantly with the material, but are in general limited.[7,8] Respirators, on the other hand, fit tightly to the face and protect against both inhalation and exhalation of fine airborne aerosols. Notwithstanding the uncertainty in the mode of transmission, the "gold standard" for personal protection among hospitals, healthcare workers, first responders, etc. is the N95 respirator, a filtering facepiece respirator

Received: January 19, 2021
Accepted: March 25, 2021

(FFR) that is intended to filter out at least 95% of airborne aerosol particles. N95 respirators were widely deployed among those at risk of exposure to high levels of virus-containing aerosols. Therefore, there was an urgent need to ensure the effectiveness of the respirators for the safety of front-line workers.

In the United States, N95 respirators are certified by the National Institute for Occupational Safety and Health (NIOSH), under the standard testing procedure for air-purifying respirators TEB-APR-STP-0059. Other countries have also established standards to certify respirators that are commonly regarded as comparable to the N95 type. For example, KN95 respirators, which are subject to China's GB2626-2006 standard, and FFP2 respirators, certified under the EN-149-2001 standard of the European Union, are expected to provide similar levels of protection against aerosols.[9] With the shortage of domestic N95 supplies, internationally sourced FFRs, including the KN95 type, were approved for use in the US under an Emergency Use Authorization (EUA) by the Food and Drug Administration (FDA). In an effort to evaluate the quality of the N95/KN95-type respirators before they were dispensed to those on the front lines of the pandemic, we tested the filtration performances of 136 such respirators with regard to their effectiveness at capturing submicron aerosols as well as their air resistance.

In general, surgical masks and respirators on the market consist of a minimum of three layers, with at least one nonwoven active filter layer in the middle that is the most efficient at capturing particles, plus two outer layers that protect the active layer(s) against mechanical abrasion, tearing, and humidity. The nonwoven active filter layer is commonly made of melt-blown polypropylene, a fibrous material comprising randomly oriented fibers with a wide diameter distribution spanning from less than one to several tens of micrometers.[10,11] Uncharged fibrous filters capture aerosols through predominantly mechanical mechanisms, such as impaction, interception, and diffusion. However, it is challenging to achieve high filtration efficiency with such filters while maintaining sufficiently low filter thickness and high porosity so that the pressure drop is small, to ensure breathability. To enhance the filtration efficiency of such filters without significantly increasing the pressure drop, electrostatic charges are commonly injected into the filter material, allowing more particles to be captured also through electrostatic mechanisms, in addition to mechanical ones.[12] Since the efficiencies of both mechanical and electrostatic particle-capture mechanisms exhibit different dependences on particle size, the overall combined filtration efficiency is nonuniform. In most filters, penetration is maximal at a certain particle size, which is referred to as the most penetrating particle size (MPPS). The particle penetration at the MPPS thus reflects a worst-case scenario in filtration performance. In mechanical filters, for example, small particles are captured predominantly through the diffusive mechanism, while large particles are collected predominantly through inertial impaction and interception mechanisms. As a result, these filters typically exhibit an MPPS around an intermediate particle size of about 300 nm. The introduction of electrostatic charges has been found to improve the filtration efficiency in the intermediate particle size range and to reduce the MPPS down to less than 100 nm.[4,13,14] This effect was also seen on electrostatically charged N-type respirators, which exhibit an MPPS of ∼50 nm.[15] Despite the increase in filtration efficiency, however, such electret filters may lose their electrostatic charges over a period of time, due to environmental factors or mishandling, for example, leading to compromised long-term performance. In this study, we investigated the effects of both mechanical and electrostatic mechanisms on the performances of FFRs, in terms of filtration efficiency and MPPS, to gain insight into the function of FFRs available on the market and their prospects for long-term performance.

EXPERIMENTAL SECTION

A total of 136 FFRs were characterized in this study. The respirators comprised a combination of N95-certified and KN95 (certification not confirmed) products that were received by our lab between April and June 2020 from multiple sources throughout the Commonwealth of Massachusetts. Each respirator was characterized for a few basic properties such as thickness and basis weight. Thickness was obtained using a micrometer (Mitutoyo 293-832, Mitutoyo Corp.) under an applied force of 0.5 N. The average thickness of the 136 respirators, including all constituent layers, was 193 ± 51 μm, and the average basis weight was 0.575 ± 0.161 g/m^2.

The aerosol filtration test procedure was designed to mimic the NIOSH testing protocol for N95 respirators with respect to pretreatment and challenge aerosols. The detection of aerosol penetration by particle size and subsequent averaging over particle counts deviated from the NIOSH protocol. The filtration setup is the same as that reported previously by our group.[16,17] The challenge aerosols were generated using the atomizer in a condensation monodisperse aerosol generator (CMAG, Model 3475, TSI Inc.), in which compressed air was bubbled through a 0.5 wt % sodium chloride solution at 2.5 L/min. The atomized solution was then dried by passage through a packed bed of silica beads and diluted with compressed air at 20 L/min, resulting in solid sodium chloride particles with a particle density of about 10^6 #/cm^3, count median mobility diameter (CMD) within the NIOSH-specified range of 75 ± 20 nm, and geometric standard deviation (GSD) smaller than 1.86.[18] Under normal testing conditions, the aerosols generated by the atomizer were charge-equilibrated using a radioactive neutralizer (TSI 3077S, TSI Inc.). A typical challenge aerosol is shown in Figure 1. The size and number distribution of the aerosols were measured with a scanning mobility particle sizer (SMPS) consisting of a differential mobility analyzer (DMA, Model 3081, TSI Inc.) and a condensation particle counter (CPC, Model 3775, TSI Inc.), which yields a count of the number of particles using an optical counter after enlarging them

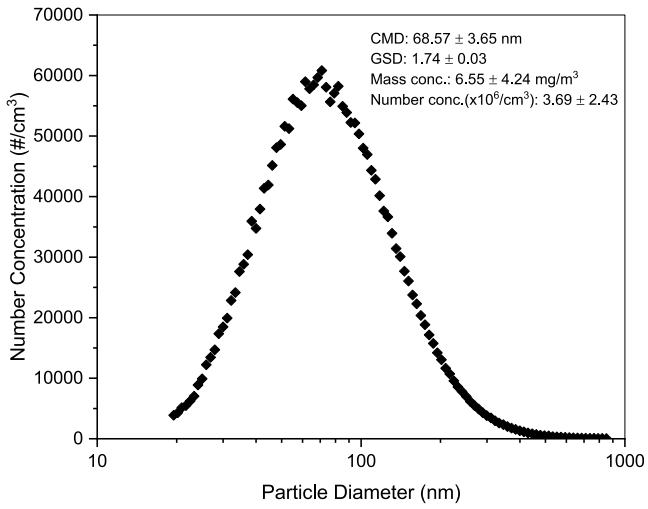

Figure 1. Typical size distribution of challenge NaCl aerosol. The inset summarizes the important properties of the challenge aerosol averaged over the 400+ tests performed in this work.

https://doi.org/10.1021/acsanm.1c00139
ACS Appl. Nano Mater. XXXX, XXX, XXX−XXX

through condensation of butanol. The particle number concentration was measured in 106 bins distributed logarithmically in particle diameters from 20 to 850 nm. A diagram of the setup of the filtration system has been reported previously.[17]

Prior to filtration tests, respirators were preconditioned at 85% humidity overnight. Three samples, cut into 3.8 cm^2 disks, were tested for each respirator type. To take into consideration the variation between individual respirators of the same type, samples were cut from three separate respirators whenever possible. Thus, the filtration test performed here applies only to the material of the FFR; it does not address differences in filter shape, flow inhomogeneities, or fit to the user. Unless indicated otherwise, characterization of samples was performed with all layers of the respirator intact. The volumetric flow rate of air was controlled to 2.2 L/min by a vacuum pump on the downstream side of the filter. The resulting face velocity at the filter was 9.6 cm/s, chosen to replicate the face velocity of the NIOSH protocol, assuming 85 L/min for a full respirator with an effective surface area of 150 cm^2.[19] The filtration test for each sample lasted 15 min, with the pressure drop (Δp) across the filter constantly monitored using a manometer (HD750, Extech Instruments). The procedure comprised two scans of the upstream aerosol size distribution with no filter sample in place, followed by insertion of the sample and five scans of the aerosol size distribution downstream of the sample. Lastly, the sample was removed and upstream aerosol was scanned two more times to monitor the stability of the upstream aerosol. Successive scans were performed at 3 min intervals. The number concentration and size distribution of the upstream aerosol were averaged over the four scans. For the downstream aerosol, measurements from the first four scans were discarded to flush out any residual particle accumulation in the system from the upstream measurements, and number concentration and size distribution were obtained from the fifth scan. The sample-to-sample variation in penetration within each respirator type was about 4%, while the Type B uncertainty was estimated to be less than 0.3%. With the particle concentration used in the tests, the 15 min of filtration time with the sample in place would result in a particle loading of only 0.055 ± 0.035 mg/cm^2. Particle penetration as a function of mobility diameter ($P(d_p)$) was determined by dividing the number concentration of the downstream aerosol in the corresponding bin by that of the upstream aerosol in the same bin. The total count penetration (P_c) was determined by dividing the total number concentration of the downstream aerosol by that of the upstream aerosol. The filtration efficiency (E_c) is $1 - P_c$.

To study the origin of observed variations in filtration performance, samples with qualitatively different penetration profiles (as described later) were selected from the 136 respirators for further analysis. As the main particle-capture media, the active middle layers of the respirators were also separated from the other layers and characterized individually. The active layers were examined under a scanning electron microscope (SEM, JOEL 6010LA, JEOL, Ltd.). The fiber diameter distribution was measured from the SEM images, using 80–150 fibers from each sample. For greater accuracy, the thickness of the active layer was also measured by examining a cross section of the layer under SEM. To minimize mechanical distortion, the samples were cut immediately after submersion in liquid nitrogen for 30 s. The samples were tested with all layers together in filtration testing. To eliminate electrostatic charges from the fibers, the samples were submerged in isopropyl alcohol (IPA, CAS 67-63-0, Sigma-Aldrich) for 2 h and dried at room temperature overnight before filtration testing. In general, charges on aerosols passing through the radioactive neutralizer would be reduced to a Boltzmann-equilibrated charge distribution; to retain electrostatic charges on the aerosol particles as generated, the neutralizer was bypassed in some tests. As a matter of nomenclature, in this work, a filter sample without IPA treatment is abbreviated OF (original filter), while an IPA-treated sample is abbreviated DF (discharged filter). As-generated particles bypassing the neutralizer are referred to as charged particles (CPs) and those having gone through the neutralizer are called neutralized particles (NPs).

RESULTS AND DISCUSSION

Penetration of N95 and KN95 Respirators. The two most commonly reported properties of face masks and respirators are filtration efficiency (alternatively, the total particle penetration) and pressure drop across the respirator, a measure of breathability. Figure 2 shows the penetration vs particle mobility diameter for three certified N95 FFRs, as measured by our protocol, along with the total count penetration and the measured pressure drop in each case. Samples from all three N95 FFRs exhibited total count penetrations of less than 3% and pressure drops below the limit of 343 Pa (35 mm of water) for N/P-type respirators under the TEB-APR-STP-0007 testing procedure.[20] At a particle size of 300 nm, a widely used reference particle size for mechanical filters,[21] penetrations through the samples were 1.71 ± 0.62, 1.53 ± 0.39, and 0.20 ± 0.04%, respectively; these values are lower than the total penetration measured for the respective FFRs. Therefore, a conservative evaluation of filtration performance for these FFRs requires testing aerosol penetration for particles smaller than 100 nm, as has been noted previously.[22]

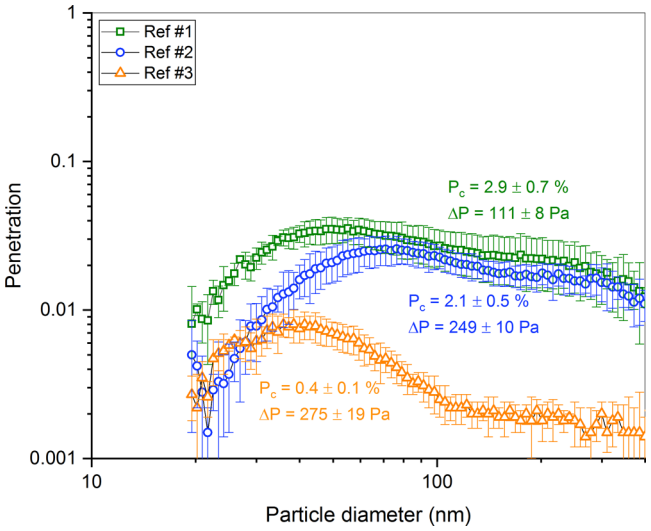

Figure 2. Example measurements of particle penetration vs particle size for three N95 reference respirators; the labels show the total particle penetration and the pressure drops for each respirator.

Similar measurements were performed for a total of 136 FFRs, including five N95 (two of which were not used as references due to uncertain provenance) and 131 KN95 respirators. Figure 3 summarizes the count penetration and the initial pressure drop of these FFRs. There are several noteworthy observations from this data. First, according to Figure 3a, about 42% of the FFRs exhibited total count penetration values below 10%, with 17% showing penetration below 5%. However, over a third of samples exhibited relatively high penetration of greater than 20%. On the other hand, almost all samples showed reasonable pressure drops, below the NIOSH limit of 343 Pa at a face velocity of 9.6 cm/s. Thus, it was immediately apparent that the KN95 FFRs were of widely varying quality and that it would be advisable to confirm the effectiveness of such devices prior to distributing them to users in the early days of the pandemic. This observation is consistent with results reported previously by Brochot et al.[23] Figure 3b shows that the initial pressure drop

https://doi.org/10.1021/acsanm.1c00139
ACS Appl. Nano Mater. XXXX, XXX, XXX−XXX

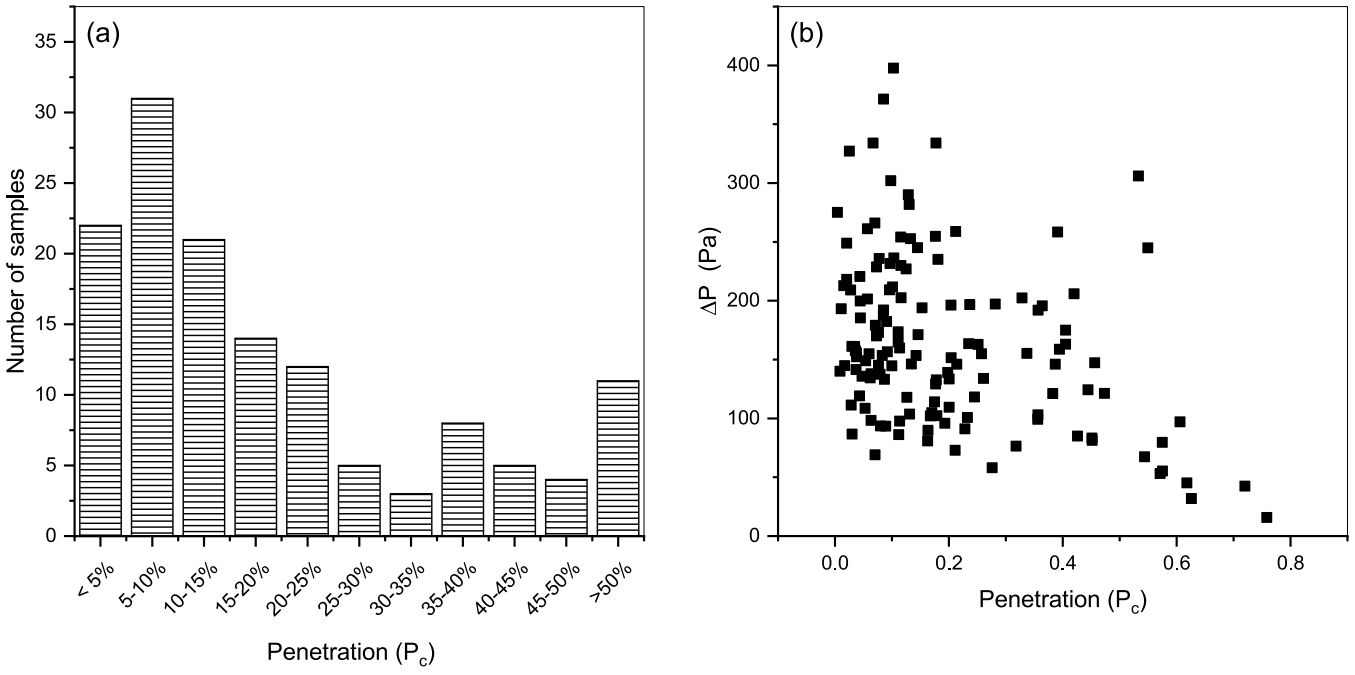

Figure 3. (a) Histogram of the total penetration for the 136 samples tested and (b) pressure drop vs count penetration.

exhibited a weak correlation with the total penetration, where high pressure drops were mainly incurred at low particle penetration.

The standard procedure for certification of N95 FFRs (TEB-APR-STP-0059) uses a specialized piece of equipment (TSI 8130 or 8130A) with photometric detection of the aerosol concentration upstream and downstream of the filter medium, rather than the size-selective particle counter used here. The result is a single value for filtration efficiency based on the amount of light scattered by the downstream aerosol over that scattered by the upstream aerosol. The TSI 8130 uses a laser with a wavelength of 780 nm. Light scattered from particles whose dimensions are less than half the wavelength of the incident laser generally follows Rayleigh scattering, which scales as the sixth power of particle diameter, d_p^6.[24] Therefore, the photometric measurement is heavily biased toward detection of the larger particles in the distribution. Thus, a significant fraction of the number of particles in the challenge aerosol is essentially invisible to the instrument. In fact, an analysis by Eninger et al. found that 68% (by number) of the challenge aerosols go undetected in the NIOSH testing protocol.[25] Comparative studies on photometric and number-based measurements of particle penetration also demonstrated that, in the case of electret filters, the photometric measurement could yield aerosol penetration values several-fold, or even orders of magnitude, lower than those measured by the number-based method.[26,27] To estimate the power-average penetration that would be recorded by a photometric measurement, we compared the light scattering intensities from the downstream and the upstream aerosols, calculated using eqs 1 and 2 [25,28]

$$I = c_n \int_0^\infty f(d_p) S_\lambda(d_p) d(d_p) \quad (1)$$

$$S_\lambda(d_p) = \frac{2\pi^5}{3\lambda^4} \left| \frac{m^2 - 1}{m^2 + 2} \right|^2 d_p^6 \quad (2)$$

where I is the total intensity of light scattered, $f(d_p)$ is the number distribution of particles by diameter in the challenge aerosol, $S_\lambda(d_p)$ is the intensity of light scattered by a particle of diameter d_p, following the scaling relationship of Rayleigh scattering, m is the refractive index of the particle relative to that of the medium, and c_n is the total aerosol number concentration. The scattering was calculated using aerosols smaller than half the wavelength of the TSI 8130 laser, which accounted for >99.8% of the test aerosols, so that Rayleigh scattering applies. The calculated power-average penetrations (P_p) are plotted as a function of the experimentally measured count penetration (P_c) in Figure 4.

As demonstrated in Figure 4, FFRs with a relatively low total count penetration exhibited $P_p < P_c$, which indicates that a significant number of penetrating particles were of small

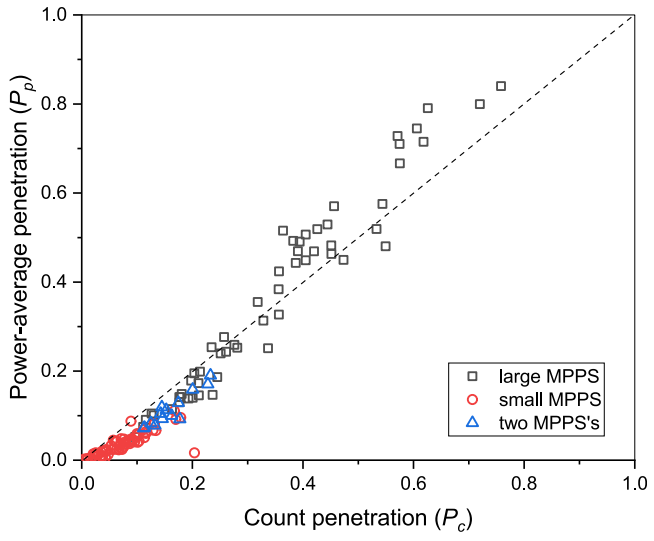

Figure 4. Parity plot of count penetration (P_c) measured by the SMPS and power-average penetration (P_p) calculated using eq 1.

https://doi.org/10.1021/acsanm.1c00139
ACS Appl. Nano Mater. XXXX, XXX, XXX−XXX

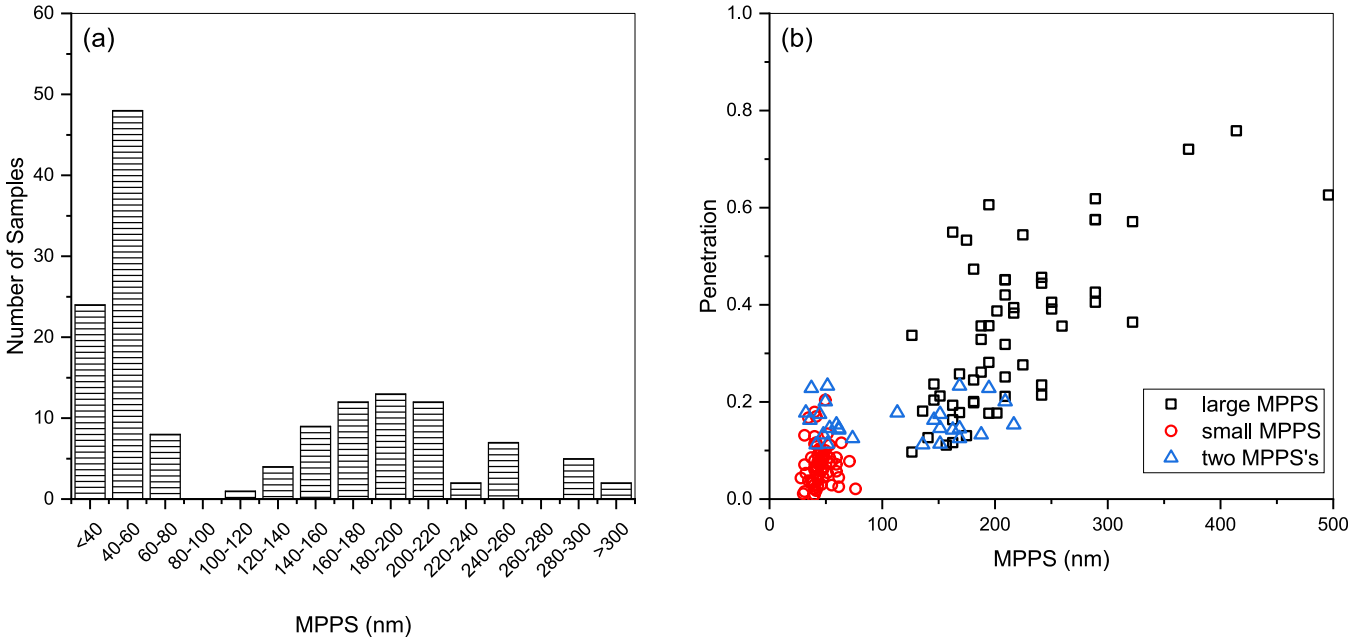

Figure 5. (a) MPPS distribution for the 136 tested respirators and (b) total count penetration vs MPPS for the three types of respirators observed in this work.

diameter and contributed relatively little to the photometric measurement. FFRs characterized by total penetration greater than about 30% exhibited $P_p > P_c$. This behavior indicates that the downstream aerosols contained larger fractions of large particles than did the upstream aerosols since light scattering intensity increases with particle size. Thus, the evaluation of penetration (or filtration efficiency) is sensitive to the method used to measure particle concentration; there is a systematic bias toward overestimation of filtration efficiency among the most efficient filters and underestimation among the least efficient filters with the photometric method.

Most Penetrating Particle Size. According to the single-fiber theory, MPPS is the result of the combined effects of several particle-capture mechanisms, whose efficiencies depend on particle size as well as filter properties.[29] A histogram of the MPPSs for all 136 samples is shown in Figure 5a. This figure suggests that the samples can be classified into two distinct groups: those with MPPS < 100 nm and those with MPPS > 100 nm. The larger MPPS is consistent with that of conventional mechanical filters, such as HEPA filters, which tend to be least effective at capturing particles of size around 300 nm. Most respirators exhibited one MPPS in either of the groups. A third group, comprising about 10% of the respirators, showed two local maxima in penetration, one each above and below 100 nm. Figure 6 illustrates the penetration profiles for representative respirators from each of these three groups. Again, similar behaviors have been observed previously among KN95 respirators.[30] Nevertheless, the coexistence of two local MPPS in the same filter is apparently not common. He et al. reported the double peak in the particle penetration profile of N95 respirators and attributed the phenomenon to the compound effect from multiple layers of the respirators.[31] A comparison between the filtration behaviors of a respirator both including all layers and with only the active layer (Figure S1) shows that the support layers did not noticeably change the penetration profile and thus could not have been the cause of the double-MPPS behavior. The three types are also distinguished in both Figures 4 and 5b by different symbols.

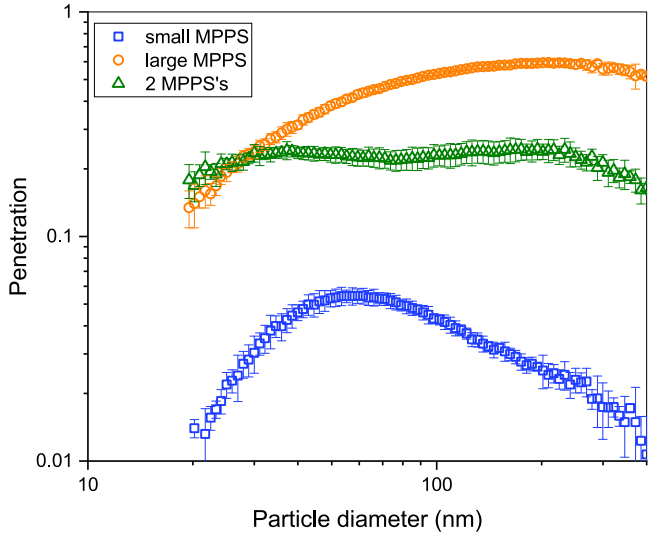

Figure 6. Penetration profiles for representative respirators from each of the three different types of behaviors observed for the FFR materials. Key: small MPPS = one MPPS that is smaller than 100 nm (blue squares); large MPPS = one MPPS that is larger than 100 nm (orange circles); and "2 MPPSs" = a local MPPS in each size range (green triangles).

Figure 5b shows the count penetration vs MPPS; for a sample with two local MPPSs, both values are plotted. The correlation between MPPS and count penetration is readily apparent. For the purposes of subsequent discussion, samples with one MPPS less than 100 nm are designated the "small MPPS" type, all of which had count penetrations lower than 20%. Samples with one MPPS greater than 100 nm exhibited varying penetrations between 10 and 80%; these respirators are designated the "large MPPS" type. Those samples with two local MPPSs, henceforth designated the "double MPPS" type, exhibited intermediate penetration around 20%. Consistent with the discussion of Figure 4, the small MPPS-type

https://doi.org/10.1021/acsanm.1c00139
ACS Appl. Nano Mater. XXXX, XXX, XXX−XXX

Table 1. Filter Properties of Selected Respirators

sample ID	thickness (μm)		basis weight (g/m^2)		fiber diameter (μm)	estimated charge density (μC/m^2)
layer(s)	all	active	all	active	active	active
respirator 1	553 ± 61	197 ± 23	181	38	5.70 ± 4.00	0.36
respirator 2	1191 ± 108	926 ± 14	406	126	5.17 ± 3.89	33.67
respirator 3	481 ± 16	288 ± 22	150	65	3.62 ± 2.38	5.74

respirators were most efficient in capturing the large particles, which could be easily detected by a photometer. On the other hand, large MPPS-type samples exhibiting high penetration allowed more large particles through the filter, resulting in greater light scattering intensity and thus higher penetration measurement by the photometric method.

Several differences in filter properties could have contributed to the variation in penetration and MPPS of the respirators. Plots of count penetration vs basis weight or the total thickness of the respirators (Supporting Information, Figures S3 and S4, respectively) indicate that the amount of fiber in the samples was not the determining factor for the different filtration behaviors described above. Since respirator filters are typically made of electret materials, it is possible that the level of electrostatic charges played a role in determining the penetration and the MPPS. It is known that the addition of electrostatic charges can not only improve the overall filtration efficiency but also significantly enhance particle capture in the size range where mechanical filtration is weak, thus resulting in smaller MPPS.[4,13] The electrostatic and mechanical mechanisms are approximately additive, so the coexistence of the two MPPSs may also be the result of an electrostatic effect that is not strong enough to improve the capture of larger aerosols as strongly as that of smaller aerosols.[32,33]

Electrostatic Effects. To understand better the effect of electrostatic charge on filtration behavior, several respirators with different penetration profiles, exhibiting different MPPS types and filtration efficiency levels, were selected for further study. Properties of the representative samples are listed in Table 1. Respirators 1 and 3 included only one nonwoven active layer, while respirator 2 had two layers of active material with a spacer in between; the values reported in Table 1 indicate the combined thickness and basis weight of the double layer for respirator 2. Figure 7 shows the SEM images of the active layers of the three respirator samples as well as the corresponding fiber diameter distributions. All samples exhibited a broad distribution of fiber diameter and branching of fibers, features typical of melt-blown fabrics. As can be seen in Table 1, the mean fiber diameters ranged from 3 to 6 μm. Among the three samples, the fiber diameter in respirator 1 appears to be particularly polydisperse. The SEM images were taken after filtration tests, so a few salt aerosol particles can be seen adhering to the fiber surfaces. The low incidence of adhered particles confirms that the particle loading in this work was too low to affect penetration or pressure drop measurements significantly. Samples treated with isopropyl alcohol (IPA) were also examined under SEM, but no visible difference from the original materials was found.

Figure 8 shows the penetration profiles of the three respirators under four different combinations of electrostatic charging on the fibers and particles: original filter with aerosol neutralized to Boltzmann charge equilibrium (OF-NP), filter discharged by IPA treatment with neutralized aerosol (DF-NP), original filter with unneutralized aerosol carrying as-generated charges (OF-CP), and discharged filter with unneutralized aerosol (DF-CP). The total count penetration and pressure drop for the 12 cases are summarized in Table 2. Comparison of the data in Tables 1 and 2 does not suggest any consistent correlation between total penetration, measured under OF-NP conditions, and physical properties of the filter such as fiber diameter, thickness, and basis weight. The samples tested under OF-NP conditions did exhibit rather different penetration profiles as a function of aerosol size. Respirator 1 (Figure 8a) was of the large MPPS type, showing an MPPS around 200 nm. Respirator 2 (Figure 8b) was of the small MPPS type, with MPPS around 30 nm and low total penetration of 2%. Respirator 3 (Figure 8c) was of the double MPPS type, showing one MPPS around 40 nm and another around 200 nm. From the penetration profiles, we highlight two observations. First, in each of the three respirators, the penetration results can be grouped into a pair with higher count penetration (25−66%), which share the DF trait, and a pair with lower count penetration (1−10%, with the notable exception of respirator 1 at 47−53%), which share the OF trait. Compared to the other two respirators, respirator 1 exhibited relatively high penetration even for the OF pair. For respirators 2 and 3, the increase in penetration after IPA treatment was accompanied by a shift of the MPPS from below 100 nm to around 200 nm. Similar observations can be made for other samples we have tested, as shown in Figure S2 and Table S2. Namely, samples with high penetration (~50%) and large MPPS (~200 nm) as OF exhibited no noticeable change in filtration performance after IPA treatment. In contrast, samples with originally low penetration (<11%) and <100 nm MPPS showed a significant increase in both penetration and MPPS as DF. In fact, all samples consistently behaved as mechanical filters after IPA treatment, characterized by high penetration (>25%) and large MPPS (around 200 nm). Since the IPA treatment serves to remove electrostatic charges from the fibers, the difference between the OF cases and the DF cases can be attributed to electrostatic effects. We thus conclude that electrostatic mechanisms play a major role in the performance of high-efficiency filters such as respirators 2 and 3, but less so in the case of low-efficiency filters such as respirator 1. Indeed, within the uncertainty of the measurement, the performance of respirator 1 appeared to be insensitive to the IPA treatment. We conclude that the fibers of respirator 1 were probably uncharged as received.

Second, within each pair of penetration results, neutralization of the aerosol particles served to increase the penetration for the original, untreated fibers (OF-CP vs OF-NP), whereas it had little effect on the IPA-treated fibers (DF-CP vs DF-NP). From this comparison, we conclude that the image charges induced on the particles by the charged fibers are important. Coulombic charge interactions also contribute to particle capture when the particles are charged. By contrast, in the absence of charges on the fibers (DF), the charging of the aerosol as generated was insufficient to affect penetration significantly. To confirm these conclusions, quantitative comparison to the penetration of particles through charged

https://doi.org/10.1021/acsanm.1c00139
ACS Appl. Nano Mater. XXXX, XXX, XXX−XXX

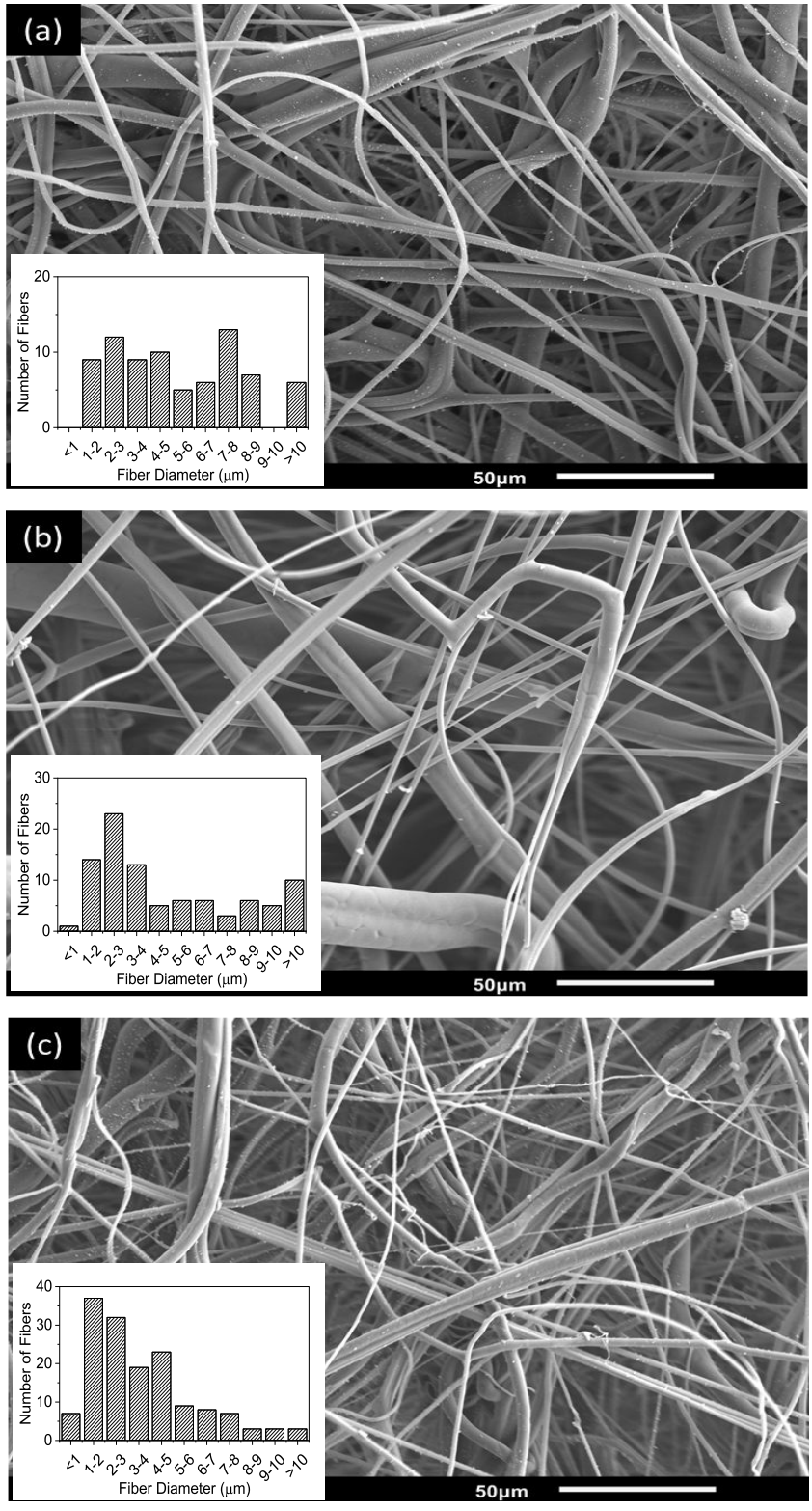

Figure 7. SEM images of the active layers from samples of (a) respirator 1, (b) respirator 2, and (c) respirator 3; the insets show the fiber diameter distributions.

and uncharged filters according to the single-fiber theory is reported next.

Penetration Modeling. To relate filtration performance to properties of the respirators, the particle penetration profiles were computed using the single-fiber theory.[29] According to this theory, particle penetration through the filtration medium is a function of the thickness (t), solidity (α), fiber diameter (d_f), and single-fiber efficiency (E_Σ) according to[34]

$$P(d_p) = 1 - E(d_p) = \exp\left(-\frac{4\alpha E_\Sigma t}{(1-\alpha)\pi d_f}\right) \quad (3)$$

https://doi.org/10.1021/acsanm.1c00139
ACS Appl. Nano Mater. XXXX, XXX, XXX−XXX

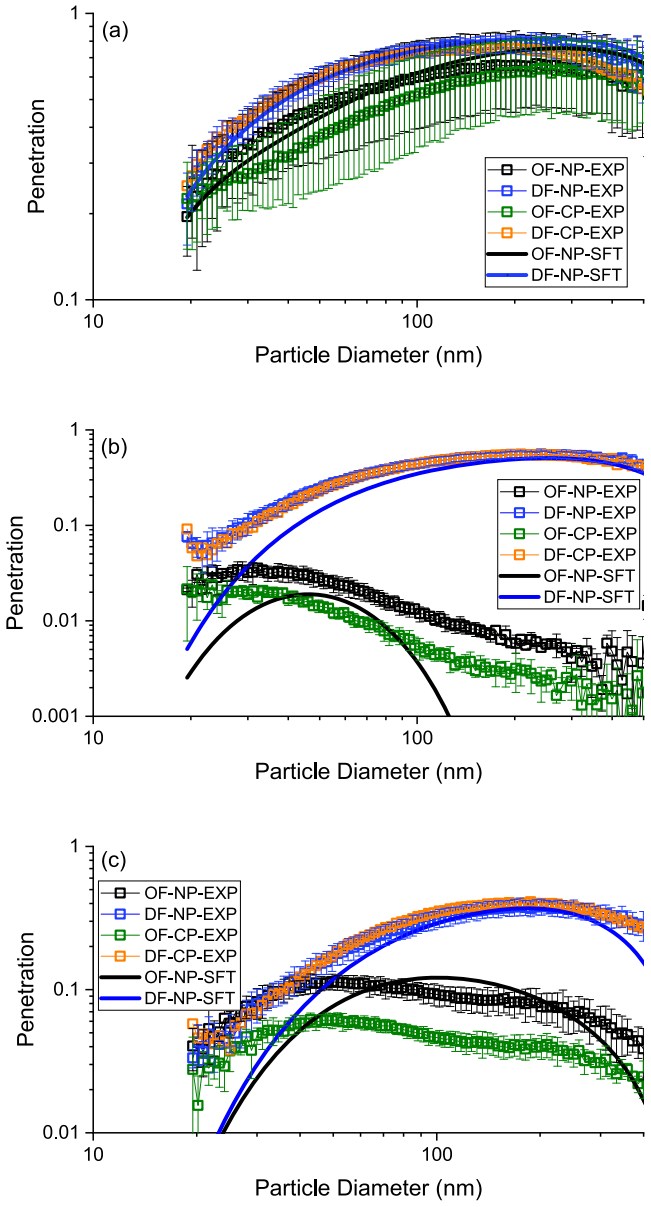

Figure 8. Experimental data (symbols, EXP) for aerosol penetration under four different combinations of electrostatic charging on the fibers and particles, and comparison with the predictions of the single-fiber theory (solid curves, STF) for original (OF-NP) and discharged (DF-NP) samples for (a) respirator 1, (b) respirator 2, and (c) respirator 3.

where $E_{\sum}$ is a function of aerosol particle diameter, among other parameters, as described below. In the absence of electrostatic interactions, the relevant mechanical particle-capture mechanisms of single-fiber efficiency are diffusion (E_D), interception (E_R), diffusion-enhanced interception (E_{DR}), and impaction (E_I), described by eqs 4−7, respectively[34]

$$E_R = \frac{(1-\alpha)R^2}{Ku(1+R)} \tag{4}$$

$$E_I = \frac{(Stk)J}{(2Ku)^2} \tag{5}$$

$$E_D = 2Pe^{-2/3} \tag{6}$$

$$E_{DR} = \frac{1.24R^{2/3}}{Ku^{1/2}Pe^{1/2}} \tag{7}$$

In these equations, Ku is the Kuwabara hydrodynamic factor, R is the ratio of particle diameter to fiber diameter, Stk is the Stokes number, and Pe is the Peclet number; J is an empirical function of α and R. The single-fiber efficiency $E_{\sum}$ may then be written approximately as the sum of the individual single-fiber efficiencies for each mechanism. Additional details of this calculation can be found in the Supporting Information as well as Hinds.[29]

When the filter is electrostatically charged, aerosols can also be collected through electrostatic interactions, comprising both the direct Coulombic interaction (E_C) between charged fibers and charged aerosols as well as induced charge interactions when only one of the two (fiber or aerosol) is charged, and the other is polarizable ($E_{i,f}$ and $E_{i,p}$), described by eqs 8−10, respectively

$$E_C = -\frac{CQ_pQ_{af}}{3\mu d_p v\varepsilon_0} \tag{8}$$

$$E_{i,f} = \left[\frac{\pi(\varepsilon_p-1)Cd_p{}^2Q_{af}{}^2}{2(\varepsilon_p+2)\mu d_f v\varepsilon_0}\right]^{1/3} \tag{9}$$

$$E_{i,p} = \left[\frac{3(\varepsilon_f-1)CQ_p{}^2}{4(\varepsilon_f+2)\pi^2\mu d_f{}^2 d_p v\varepsilon_0}\right]^{1/2} \tag{10}$$

where Q_p is the charge on the particle and Q_{af} is the specific charge per unit area on the fiber. ε_p and ε_f are the dielectric constants of the particle and the fiber, respectively, ε_0 is the permittivity of free space, μ is the air viscosity, v is the face velocity, and C is the Cunningham correction factor. Here, the total single-fiber efficiency $E_{\sum}$ includes the efficiencies of both mechanical and electrostatic mechanisms. The reader is referred to Kraemer and Johnstone and to Rodrigues et al. for detailed discussions of the efficiencies of these mechanisms.[33,35] The aerosol particle charge distribution, $W(Q_p)$, can be taken into account using the method of Lathrache et al.,

Table 2. Filtration Performances of Respirators 1−3 under Different Treatment Conditions

sample ID		OF-NP	DF-NP	OF-CP	DF-CP
respirator 1	P	0.53 ± 0.18	0.66 ± 0.05	0.47 ± 0.16	0.66 ± 0.07
	ΔP_0 (mmH_2O)	9.9 ± 2.2	8.8 ± 2.0	8.5 ± 1.8	13.8 ± 5.5
respirator 2	P	0.02 ± 0.00	0.35 ± 0.04	0.01 ± 0.00	0.35 ± 0.04
	ΔP_0 (mmH_2O)	17.7 ± 0.8	17.5 ± 1.3	20.4 ± 1.9	21.9 ± 1.9
respirator 3	P	0.10 ± 0.02	0.25 ± 0.04	0.05 ± 0.01	0.27 ± 0.02
	ΔP_0 (mmH_2O)	15.8 ± 1.2	17.0 ± 0.9	17.9 ± 2.0	18.5 ± 1.0

https://doi.org/10.1021/acsanm.1c00139
ACS Appl. Nano Mater. XXXX, XXX, XXX−XXX

shown in eq 11.[13] Even when in charge equilibrium, the larger particles can have non-negligible charge. The charge distribution of particles in Boltzmann equilibrium has been reported elsewhere.[36] Then, eq 3 for penetration becomes

$$P(d_p) = \sum_{Q_p=-6e}^{Q_p=+6e} W(Q_p)P(d_p, Q_p) \quad (11)$$

where E_Σ now depends on both aerosol particle size and charge and e is the electron charge.

For comparison of the single-fiber theory to experiments, we first evaluated the penetration as a function of particle diameter assuming no electrostatic charges on the fiber ($Q_{af} = 0$) and compared these to the experimental data for DF-NP samples using the properties reported in Table 1 for each respirator and the known Boltzmann equilibrium charge distribution for the aerosol. The results are shown with the blue solid lines in Figure 8; the theoretical predictions are remarkably good, given that there are no adjustable parameters. This agreement confirms that electrostatics are not necessary to explain the performance of any of the respirators treated by IPA. The good fitting of the DF-NP data, together with the unchanged filtration behaviors upon IPA treatment of low-efficiency samples, indicates that the FFRs with high penetration values and large MPPSs can be characterized solely as mechanical filters. Next, we evaluated the penetration as a function of particle diameter assuming electrostatic charges on the fiber. Since the different single-fiber filtration mechanisms are approximately additive, the adjustable parameter, Q_{af}, was determined by a linear least-squares fit between the electrostatic effect in the single-fiber theory, $-4\alpha t(E_c + E_{i,f} + E_{i,p})/(1 - \alpha)\pi d_f$, and the log difference between the experimentally measured penetrations for the OF-NP and DF-NP samples ($\ln(P_{OF\text{-}NP}/P_{DF\text{-}NP})$). Penetration profiles of respirators 4−8 in the Supporting Information were fitted similarly using the single-fiber theory.

Tables 1 and S1 show the resulting estimates of the specific charge for each respirator. The values reported here are in the same range as those found elsewhere.[37−39] As expected, the estimated charge densities on respirators 1, 6, and 7 were very small. In general, the charge density correlates with the difference between OF and DF performances. While the theoretical calculations are in agreement with the experimental measurements for mechanical filters, the single-fiber theory does not model the difference between original and IPA-treated fibers with high accuracy. Although the model reflects the general trend of decreasing penetration and MPPS with increasing specific charge on the fibers, it predicts smaller shifts in MPPS than those observed experimentally. The double-MPPS phenomenon is also not captured by the model. Therefore, a better understanding of the electrostatic effects of the filtration process, particularly the extrapolation from single-fiber behavior to filter behavior, is needed.

CONCLUSIONS

In this study, the nanoparticle filtration behaviors of N95 and KN95 FFRs were evaluated through a survey of 136 respirators acquired due to an emergency use authorization for internationally sourced FFRs during the pandemic. The FFR samples exhibited a startlingly large variation in effectiveness, with 42% of the respirators showing better than 10% penetration but roughly 35% showing worse than 20% penetration. To understand why, several representative samples were examined in greater detail. We found strong evidence for a lack of electrostatic filtration mechanisms in the underperforming FFRs, which relied solely on mechanical filtration, and were characterized by high penetration and large MPPS, around 200 nm vs less than 100 nm for high-performing FFRs. The correlation between MPPS and penetration would furthermore be expected to result in an underestimation of penetration for the FFRs at the high end of performance when characterized for filtration efficiency photometrically. For FFRs that rely on active layers of melt-blown polypropylene, we conclude that a better appreciation is needed of methods to ensure the generation and retention of electrostatic charges on the fibers during various stages of the supply chain, including production, transportation, storage, distribution, and use. Additionally, alternative filtration media that provide the desired level of filtration performance without reliance on electrostatic mechanisms could offer better reliability in aerosol protection to the end user.

ASSOCIATED CONTENT

Supporting Information

The Supporting Information is available free of charge at https://pubs.acs.org/doi/10.1021/acsanm.1c00139.

(I) Active layer and all-layer comparison; (II) additional IPA treatment results; (III) additional information for single-fiber efficiency calculations; and (IV) penetration vs basis weight and thickness (PDF)

AUTHOR INFORMATION

Corresponding Author

Gregory C. Rutledge − *Department of Chemical Engineering, Massachusetts Institute of Technology, Cambridge, Massachusetts 02139, United States;* orcid.org/0000-0001-8137-1732; Email: rutledge@mit.edu

Authors

Junli Hao − *Department of Chemical Engineering, Massachusetts Institute of Technology, Cambridge, Massachusetts 02139, United States;* orcid.org/0000-0001-6903-1057

Rachel Passos de Oliveira Santos − *Department of Chemical Engineering, Massachusetts Institute of Technology, Cambridge, Massachusetts 02139, United States; Department of Biosystems Engineering, University of São Paulo, São Paulo 13630-000, Brazil;* orcid.org/0000-0003-1320-5550

Complete contact information is available at: https://pubs.acs.org/10.1021/acsanm.1c00139

Notes

The authors declare no competing financial interest.

ACKNOWLEDGMENTS

The authors are grateful to Michael Rein, Jimmy Nguyen, and Kristen Mulherin of the Advanced Functional Fabrics of America (AFFOA), William Herzog and Mordechai Rothschild of MIT Lincoln Laboratory, and Ramaswamy Nagarajan and Arlene Parquette of the University of Massachusetts at Lowell for numerous enlightening discussions during the execution of this work. Partial financial support for this work was provided by the Commonwealth of Massachusetts,

through the Massachusetts Life Sciences Center (MLSC) on behalf of the Massachusetts Manufacturing Emergency Response Team (M-ERT), and by a generous gift from M. M. Chen. The authors would also like to thank the Executive Office of Health and Human Services (EOHHS) of Massachusetts, the Massachusetts Emergency Management Agency (MEMA), and the numerous healthcare workers and first responders who have worked diligently to protect our community during the COVID-19 pandemic, shared their experience and materials with us, and placed their trust in our science.

REFERENCES

(1) CDC. Science Brief: SARS-CoV-2 and Potential Airborne Transmission. https://www.cdc.gov/coronavirus/2019-ncov/science/science-briefs/scientific-brief-sars-cov-2.html (accessed Nov. 3, 2020).
(2) WHO. Modes of Transmission of Virus Causing COVID-19: Implications for IPC Precaution Recommendations. https://www.who.int/news-room/commentaries/detail/modes-of-transmission-of-virus-causing-covid-19-implications-for-ipc-precaution-recommendations (accessed Nov. 3, 2020).
(3) Tang, S.; Jones, R. M.; Tan, Q.; Ji, J. S.; Li, N.; Shen, J.; Lv, Y.; Pan, L.; Ding, P.; Wang, X.; Wang, Y.; Macintyre, C. R.; et al. Aerosol Transmission of SARS-CoV-2? Evidence, Prevention and Control. *Environ. Int.* **2020**, *144*, No. 106039.
(4) Eninger, R. M.; Honda, T.; Adhikari, A.; Heinonen-Tanski, H.; Reponen, T.; Grinshpun, S. A. Filter Performance of N99 and N95 Facepiece Respirators against Viruses and Ultrafine Particles. *Ann. Occup. Hyg.* **2008**, *52*, 385−396.
(5) Liu, Y.; Ning, Z.; Chen, Y.; Guo, M.; Liu, Y.; Gali, N. K.; Sun, L.; Duan, Y.; Cai, J.; Westerdahl, D.; Liu, X.; Xu, K.; Ho, K. F.; Kan, H.; Fu, Q.; Lan, K. Aerodynamic Analysis of SARS-CoV-2 in Two Wuhan Hospitals. *Nature* **2020**, *582*, 557−560.
(6) CDC. Considerations for Wearing Masks. https://www.cdc.gov/coronavirus/2019-ncov/prevent-getting-sick/cloth-face-cover-guidance.html (accessed Nov. 3, 2020).
(7) Zhao, M.; Liao, L.; Xiao, W.; Yu, X.; Wang, H.; Wang, Q.; Lin, Y. L.; Kilinc-Balci, F. S.; Price, A.; Chu, L.; Chu, M. C.; Chu, S.; Cui, Y. Household Materials Selection for Homemade Cloth Face Coverings and Their Filtration Efficiency Enhancement with Triboelectric Charging. *Nano Lett.* **2020**, *20*, 5544−5552.
(8) Zangmeister, C. D.; Radney, J. G.; Vicenzi, E. P.; Weaver, J. L. Filtration Efficiencies of Nanoscale Aerosol by Cloth Mask Materials Used to Slow the Spread of SARS-CoV-2. *ACS Nano* **2020**, *14*, 9188−9200.
(9) 3M. Comparison of FFP2, KN95, and N95 and Other Filtering Facepiece Respirator Classes, 2020.
(10) Ullah, S.; Ullah, A.; Lee, J.; Jeong, Y.; Hashmi, M.; Zhu, C.; Joo, K. I.; Cha, H. J.; Kim, I. S. Reusability Comparison of Melt-Blown vs Nanofiber Face Mask Filters for Use in the Coronavirus Pandemic. *ACS Appl. Nano Mater.* **2020**, *3*, 7231−7241.
(11) Zhou, S. S.; Lukula, S.; Chiossone, C.; Nims, R. W.; Suchmann, D. B.; Ijaz, M. K. Assessment of a Respiratory Face Mask for Capturing Air Pollutants and Pathogens Including Human Influenza and Rhinoviruses. *J. Thorac. Dis.* **2018**, *10*, 2059−2069.
(12) Wang, C.-S. Electrostatic Forces in Fibrous Filters - A Review. *Powder Technol.* **2001**, *118*, 166−170.
(13) Lathrache, R.; Fissan, H. J.; Neumann, S. Deposition of Submicron Particles on Electrically Charged Fibers. *J. Aerosol Sci.* **1986**, *17*, 446−449.
(14) Martin, S. B., Jr.; Moyer, E. S. Electrostatic Respirator Filter Media: Filter Efficiency and Most Penetrating Particle Size Effects. *Appl. Occup. Environ. Hyg.* **2000**, *15*, 609−617.
(15) Rengasamy, S.; Miller, A.; Vo, E.; Eimer, B. C. Filter Performance Degradation of Electrostatic N95 and P100 Filtering Facepiece Respirators by Dioctyl Phthalate Aerosol Loading. *J. Eng. Fibers Fabr.* **2013**, *8*, 62−69.
(16) Hao, J.; Chattopadhyay, S.; Rutledge, G. C. Chemical Separation in a Binary Liquid Aerosol by Filtration Using Electrospun Membranes. *Chem. Eng. J.* **2020**, *382*, No. 122924.
(17) Chattopadhyay, S.; Hatton, T. A.; Rutledge, G. C. Aerosol Filtration Using Electrospun Cellulose Acetate Fibers. *J. Mater. Sci.* **2016**, *51*, 204−217.
(18) NIOSH. Procedure No. TEB-APR-STP-0059, Revision 3.2. Determination of Particulate Filter Efficiency Level for N95 Series Filters against Solid Particulates for Non-Powered, Airpurifying Respirators Standard Testing Procedure (STP), 2019.
(19) Rengasamy, S.; Shaffer, R.; Williams, B.; Smit, S. A Comparison of Facemask and Respirator Filtration Test Methods. *J. Occup. Environ. Hyg.* **2017**, *14*, 92−103.
(20) NIOSH. Procedure No. TEB-APR-STP-0007, Revision 2.3. Determination of Inhalation Resistance Test, Air-Purifying Respirators Standard Testing Prcedure (STP), 2019.
(21) Mostofi, R.; Wang, B.; Haghighat, F.; Bahloul, A.; Jaime, L. Performance of Mechanical Filters and Respirators for Capturing Nanoparticles - Limitations and Future Direction. *Ind. Health* **2010**, *48*, 296−304.
(22) Bałazy, A.; Toivola, M.; Reponen, T.; Podgórski, A.; Zimmer, A.; Grinshpun, S. A. Manikin-Based Performance Evaluation of N95 Filtering-Facepiece Respirators Challenged with Nanoparticles. *Ann. Occup. Hyg.* **2006**, *50*, 259−269.
(23) Brochot, C.; Saidi, M. N.; Bahloul, A. Qualitative Knowledge of Filtering Facepiece Respirators for Filtration Performance Tests during the COVID-19 Pandemic. *J. Int. Soc. Respir. Prot.* **2020**, *37*, 94−107.
(24) Sorensen, C. M.; Gebhart, J.; O'Hern, T. J.; Rader, D. J. Optical Measurement Techniques: Fundamentals and Applications.. In *Aerosol Measurement: Principles, Techniques, and Applications*; Kulkarni, P.; Baron, P. A.; Willeke, K., Eds.; John Wiley & Sons, Inc., 2011; pp 269−312.
(25) Eninger, R. M.; Honda, T.; Reponen, T.; McKay, R.; Grinshpun, S. A. What Does Respirator Certification Tell Us About Filtration of Ultrafine Particles. *J. Occup. Environ. Hyg.* **2008**, *5*, 286−295.
(26) Rengasamy, S.; Miller, A.; Eimer, B. C. Evaluation of the Filtration Performance of NIOSH-Approved N95 Filtering Facepiece Respirators by Photometric and Number-Based Test Methods. *J. Occup. Environ. Hyg.* **2011**, *8*, 23−30.
(27) Li, L.; Zuo, Z.; Japuntich, D. A.; Pui, D. Y. H. Evaluation of Filter Media for Particle Number, Surface Area and Mass Penetrations. *Ann. Occup. Hyg.* **2012**, *56*, 581−594.
(28) Sinclair, D.; La Mer, V. K. Light Scattering as a Measure of Particle Size in Aerosols. The Production of Monodisperse Aerosols. *Chem. Rev.* **1949**, *44*, 245−267.
(29) Hinds, W. C. *Aerosol Technology: Properties, Behavior, and Measurement of Airborne Particles*, 2nd ed.; John Wiley & Sons, Inc.: New York, 1999.
(30) Brochot, C.; Saidi, M. N.; Bahloul, A. How Effective Is the Filtration of 'KN95' Filtering Facepiece Respirators During the COVID-19 Pandemic? *Ann. Work Exposures Health* **2020**, 1−9.
(31) He, X.; Reponen, T.; McKay, R.; Grinshpun, S. A. Effect of Particle Size on the Performance of an N95 Filtering Facepiece Respirator and a Surgical Mask at Various Breathing Conditions. *Aerosol Sci. Technol.* **2013**, *47*, 1180−1187.
(32) Romay, F. J.; Liu, B. Y. H.; Chae, S. J. Experimental Study of Electrostatic Capture Mechanisms in Commercial Electret Filters. *Aerosol Sci. Technol.* **1998**, *28*, 224−234.
(33) Kraemer, H. F.; Johnstone, H. F. Collection of Aerosol Particles in Presence of Electrostatic Fields. *Ind. Eng. Chem.* **1955**, *47*, 2426−2434.
(34) Yeh, H.-C.; Liu, B. Y. H. Aerosol Filtration by Fibrous Filters - I. Theoretical. *J. Aerosol Sci.* **1974**, *5*, 191−204.
(35) Rodrigues, M. V.; Barrozo, M. A. S.; Gonçalves, J. A. S.; Coury, J. R. Effect of Particle Electrostatic Charge on Aerosol Filtration by a Fibrous Filter. *Powder Technol.* **2017**, *313*, 323−331.

https://doi.org/10.1021/acsanm.1c00139
ACS Appl. Nano Mater. XXXX, XXX, XXX−XXX

(36) *Series 3080 Electrostatic Classifiers: Operation and Service Manual*; TSI Inc., 2009; p B-10.
(37) Siag, A. M.; Tennal, K. B.; Mazumder, M. K. Determination of Fiber Charge Density of Electret Filters. *Part. Sci. Technol.* **1994**, *12*, 351−365.
(38) Nifuku, M.; Zhou, Y.; Kisiel, A.; Kobayashi, T.; Katoh, H. Charging Characteristics for Electret Filter Materials. *J. Electrostat.* **2001**, *51*−*52*, 200−205.
(39) Yim, W.; Cheng, D.; Patel, S. H.; Kou, R.; Meng, Y. S.; Jokerst, J. V. KN95 and N95 Respirators Retain Filtration Efficiency despite a Loss of Dipole Charge during Decontamination. *ACS Appl. Mater. Interfaces* **2020**, *12*, 54473−54480.

https://doi.org/10.1021/acsanm.1c00139
ACS Appl. Nano Mater. XXXX, XXX, XXX−XXX